

A computational investigation of the effects of swirl ratio and injection pressure on wall heat transfer in a light-duty diesel engine

Federico Perini (federico.perini@gmail.com), Adam B. Dempsey, Rolf D. Reitz
University of Wisconsin-Madison

Dipankar Sahoo, Paul C. Miles
Sandia National Laboratories

Benjamin R. Petersen
Ford Motor Company

ABSTRACT

In a recent study quantitative measurements were presented of in-cylinder spatial distributions of mixture equivalence ratio in a single-cylinder light-duty optical diesel engine, operated with a non-reactive mixture at conditions similar to an early injection low-temperature combustion mode. In the experiments a planar laser-induced fluorescence (PLIF) methodology was used to obtain local mixture equivalence ratio values based on a diesel fuel surrogate (75% n-heptane, 25% iso-octane), with a small fraction of toluene as fluorescing tracer (0.5% in mass). Significant changes in the mixture's structure and composition at the walls were observed due to increased charge motion at high swirl and injection pressure levels. This suggested a non-negligible impact on wall heat transfer and, ultimately, on efficiency and engine-out emissions. In this work, the extensive and quantitative local information provided by the PLIF experiments was used as the reference for assessing the accuracy of the CFD modeling of the engine. The KIVA3V-ERC code was used, with a sector mesh featuring high spatial resolution (about 0.1 cm). A compressible model for the extended piston and connecting rod assembly was introduced, and observed to significantly improve modeling of motored engine operation. The validation was then further extended by comparison with measured in-cylinder equivalence ratio distributions over a broad parameter range, and with measured average pressure and apparent heat release rate traces. Finally, an analysis of the effects of varying fuel injection pressures (500 - 2000 bar) and nominal swirl ratios (1.55 – 4.5) on the heat losses caused by different flow fields at the liner and piston bowl walls was conducted. The results showed the sensitivity of the combustion timing to swirl- or injection-induced wall heat transfer, and its interaction with equivalence ratio stratification.

INTRODUCTION

During recent years, increasing demand for fossil fuels and environmental sustainability concerns have motivated research

in the study of new combustion concepts for internal combustion engine operation. Direct-injected, compression ignition (DICI) combustion is of much interest due to its high energy conversion efficiency and robust operation for various engine sizes and loads [1]. However, stricter emission regulations require engine manufacturers to introduce complex and expensive after-treatment systems to reduce the nitrogen oxide (NO_x) and particulate matter (PM) emissions [2] that arise in conventional diesel combustion due to locally high combustion temperatures and fuel-rich mixture regions within the spray jet. Newer combustion strategies, such as partially-premixed compression ignition (PPCI), aim at reducing pollutant emissions in-cylinder while still maintaining a high thermal conversion efficiency [3]. However, it has been shown that excessive mixture stratification can lead to non-negligible presence of overly rich ($\phi > 1.3$) or overly lean ($\phi < 0.4$) equivalence ratio zones that undergo incomplete oxidation under highly dilute, low-temperature combustion conditions, causing significant unburned hydrocarbons (UHC) and carbon monoxide (CO) emissions [4,5].

The investigation of PPCI combustion in an optically accessible light-duty diesel engine has been object of a number of experimental studies [6-11]. These experimental campaigns have provided quantitative insight into the interactions between charge motion, engine geometry and fuel sprays, and represent a unique reference to validate computational predictions on a local basis. For example, a previous modeling study [9] has shown that the simulation of overly-lean mixture regions at the start of combustion is crucial for correctly predicting unburned hydrocarbons and carbon monoxide emissions, when operating with high EGR rates and very low loads.

A recent experimental study by Sahoo et al. [11] has shown that port-induced increases in swirl ratio significantly affect the mixing process. Both the amount of premixed combustible zones with equivalence ratios ranging between $0.5 \leq \phi \leq 1.0$, and the quantity of overly-lean mixture zones, especially in the squish volume and in the upper central portion of the combustion chamber regions, are increased with increasing

swirl. In the study it was also observed that increasing injection pressures would substantially deteriorate the mixing process. More concentrated fuel-lean and fuel-rich mixture zones were observed especially in the squish volume and in the upper central region of the cylinder, resulting in lower heat release peaks and increased UHC and CO emissions.

The focus of this work was to assess and validate the local predictive capability of detailed CFD modeling of the Sandia-GM light-duty optical-access engine, and to exploit the model to analyze the impact of swirl ratio, injection pressure, and injection-generated charge motion on wall heat transfer for low-temperature combustion. The computational model validation, continuing from a previous work [9], was extended by introducing a static mechanical compressibility model for the extended piston and connecting rod assembly of the optical engine, to be described below. The simulation results were compared to the extensive measurements of Sahoo et al. [10,11] that provided quantitative local distributions of equivalence ratios at three different planes in the combustion chamber for a total of seven operating conditions featuring different injection pressures and swirl ratios.

The results showed that the model was able to predict well the equivalence ratio distributions at the three measurement planes before ignition, also resulting in a very good match of the combustion timing. A parameter analysis based on variation of swirl ratio and injection pressure then showed the crucial effect of the swirl- and jet-induced motions at the cylinder walls to the overall heat transfer and combustion development. It is shown that, at high injection pressures, this effect combined with mixture penetration in the squish and crevice volumes, can lead to misfiring conditions. Finally, the model reveals the closely coupled interactions between the local in-cylinder flow field and the mixture penetration into the squish region. This suggests that further work should focus on modeling the full geometrical details of the combustion chamber.

EXPERIMENTAL MEASUREMENTS OF LOCAL EQUIVALENCE RATIOS

The experimental study of detailed local equivalence ratios by Sahoo et al. [11] was adopted as the reference for validating the computational models used in this work. Measurements were made on a single-cylinder, optically accessible diesel engine, derived from the current production GM four cylinder 1.9L light duty engine. The research engine, as represented in Figure 1, was equipped with an extended piston assembly, where a fused-silica piston top retained the full geometrical details of the metal piston, including valve recesses. The top ring-land crevice height was greater than the one in the production piston, but two gapless compression rings were installed to reduce blow-by. A Bosch CRIP2.2 injector was mounted vertically, and aligned with the cylinder axis; the injector holes' protrusion into the combustion chamber was of about 0.3 mm below the firedeck. A full description of the

experimental engine and injection system setup can be found in [11], while a summary of the main engine details is also reported in Table 1.

The experimental PLIF measurements of local equivalence ratios were carried out with a non-reacting charge of pure nitrogen, whose initial conditions were set to match intake flow rate and temperature at TDC of the reference combustor case's operating conditions [9]. This reference condition featured a high EGR ratio, corresponding to an intake oxygen molar fraction of 10%, and a swirl ratio $R_s = 2.20$. A comparison of the two baseline operating conditions is reported in Table 2.

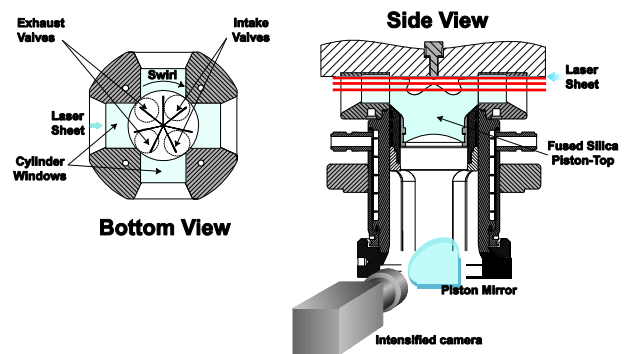


Figure 1 – Schematic representing the optical access engine setup, including laser sheet locations and camera viewing direction (from [11]).

Table 1. Main engine and experimental setup specifications for the Sandia optical-access light duty engine

Engine specifications	
Bore x stroke [mm]	82.0 x 90.4
Unit displacement [cm ³]	477.2
Compression ratio	16.38 : 1
Squish height at TDC [mm]	0.88
Bosch CRIP 2.2 Injector	
Sac volume [mm ³]	0.23
Number of holes	7
Included angle [deg]	149
Hole diameter [mm]	0.14
Hole protrusion [mm]	0.3
Fuel properties	
Composition [mole fractions]	75% nC ₇ H ₁₆
	25% iC ₈ H ₁₈
Fluorescent tracer [mass fraction]	0.5% C ₇ H ₈
Equivalent Cetane Number	47

An extensive set of 7 cases featured different port-induced swirl ratios ranging from $R_s = 1.55$ up to $R_s = 4.50$, and different injection pressures from $p_{inj} = 500$ bar up to $p_{inj} = 1220$ bar. The delivered amount of fuel was kept approximately constant for all cases by maintaining a fixed engine load. Local equivalence ratio values were derived from planar laser-induced fluorescence images, according to the methodology reported in detail in [10]. The images were obtained at three different horizontal plane positions in the combustion chamber, as represented in Figure 2: plane P1 approximately bisected the squish volume height; plane P2 was placed at the piston bowl rim edge, and finally plane P3 was placed deep into the piston bowl volume, at its maximum radius position. Measurements were taken at different crank angles values, starting from immediately after the start of injection and up to -5 degrees aTDC, i.e., immediately before the main ignition event timing: $CA = [-17.5, -15.0, -12.5, -10.0, -7.5, -5.0]$ deg aTDC. A detailed specification of the locations of the three planes at every crank angle can be found in [11].

Measurements made under the corresponding fired operating conditions showed that increasing the swirl ratio by throttling the intake port resulted in higher peak heat release rates. The PLIF measurements gave evidence that a greater mass of fuel was premixed to near-stoichiometric equivalence ratios; however, a greater amount of overly-lean mixture was also observed to be formed especially in the squish region and in the upper central portion of the combustion chamber where the tangential velocity is lower. This consequently led to increased UHC emissions, even if engine-out CO was diminished. Increasing the injection pressure rather than the swirl ratio did not help to improve the mixing process: greater amounts of overly lean mixture were observed especially in the near-nozzle region and within the squish volume. In addition to the overly-lean mixture, the squish volume also contained a greater amount of fuel-rich mixture extending almost up to the cylinder liner.

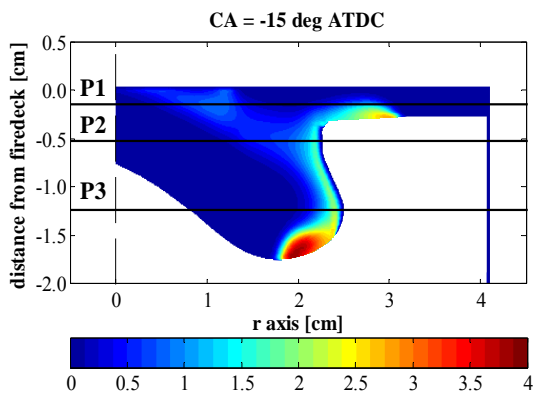


Figure 2. Horizontal plane positions of PLIF measurements at $CA = -15^\circ$ ATDC. P1 = squish volume plane; P2 = piston bowl rim plane; P3 = inner piston bowl plane. Contours represent simulated equivalence ratio (KIVA) at $R_s = 2.20$.

Table 2. Operating conditions details for both the reacting and non-reacting cases. Parameter sweeps include swirl ratio values $R_s = \{1.55, 2.2, 3.5, 4.5\}$ and injection pressures $p_{inj} = \{500, 860, 1220\}$ bar.

	Non-reacting mixture	Reacting mixture
Intake charge composition [mole fractions]	100% N ₂	10% O ₂ 81% N ₂ 9% CO ₂
Intake pressure [bar]	1.5	
Intake temperature [K]	300	372
Engine speed [rpm]	1500	
IMEP [bar]	---	3.0
Global equiv. ratio [-]	---	0.3
Injected fuel mass [g]	0.0088	0.0088
Start of Injection [deg]	$-23.0 \pm 0.1, -23.3 \pm 0.1$	
Parameter sweeps:	$R_s = 1.55, p_{inj} = 860$ bar $*R_s = 2.20, p_{inj} = 860$ bar $R_s = 3.50, p_{inj} = 860$ bar $R_s = 4.50, p_{inj} = 860$ bar $R_s = 2.20, p_{inj} = 500$ bar $R_s = 2.20, p_{inj} = 1220$ bar *baseline case	

This led to greater equivalence ratio stratification, and caused deterioration of engine-out emissions, especially increases in UHC and CO. The PLIF images thus showed how much the local mixing in the squish volume and in the upper central region of the piston bowl affects the combustion event, and rules over pollutant formation. The variety of operating conditions tested provided a unique benchmark for assessing the accuracy of multidimensional computational models that can eventually be used to simulate additional conditions, and help optimize engine operating points. In the following paragraphs, the computational modeling of the light-duty optical engine and its validation details are discussed.

COMPUTATIONAL MODELING

The computational model was built using KIVA3V-ERC, a customized version of the KIVA3V CFD code [12,13]. Many sub-models have been implemented in this version of the code, to increase its predictive capabilities, especially for fuel spray and combustion chemistry modeling. A summary of the models used for the Sandia GM optical access engine is reported in Table 3.

In the previous study of ref. [9], the use of different grid resolutions showed that an average spatial resolution of at least 1.0 mm was needed to achieve an acceptable prediction of the spray structure and of the associated local equivalence

Table 3. Main submodels activated in the KIVA3V-ERC code for modeling the Sandia-GM optical engine.

Phenomenon	Submodel
Spray breakup	KH-RT instability, Beale and Reitz [16]
Near-nozzle flow	Gas-jet theory, Abani et al. [18]
Droplet collision	O'Rourke model [12] with ROI (radius-of-influence), [18]
Wall film	O'Rourke and Amsden [19]
Evaporation	Discrete multi-component fuel, Ra and Reitz [20]
Turbulence	RNG k- ϵ , Han and Reitz [21]
Combustion	Detailed chemical kinetics with sparse analytical Jacobian, Perini et al. [23]
Reaction kinetics	Reduced PRF mechanism, Ra and Reitz [22]

ratio distribution. Similar resolution is used in the present work.

In this work, the validation has been extended by considering additional experimental measurements at different injection pressures. Furthermore, in order to make the computational model also suitable to simulate fired engine operation, elasticity effects on the extended piston and connecting rod assembly have been studied, as it had been shown that even fitting the engine grid to an effective, non-geometrical compression ratio was not enough to correctly match the peak pressure at TDC during motored engine operation.

Compressible piston-connecting rod assembly model

In the previous modeling studies [9, 14] the engine's computational grid volume was artificially increased by adding a number of cell layers in the crevice region in order to reduce the geometrical compression ratio, $CR = 16.38$, to a reduced "practical" effective value of about 15.7 (cf., comparison of the two grids in Figure 3). This procedure allowed the measured average in-cylinder pressure curve of the motored engine to be well-matched, even if peak pressure values around TDC were overestimated. For conventional metal engines it is acknowledged that this approach is better than simply adjusting the squish height at TDC. In this way, it is possible to take into account effects of both the combustion chamber deformation and charge

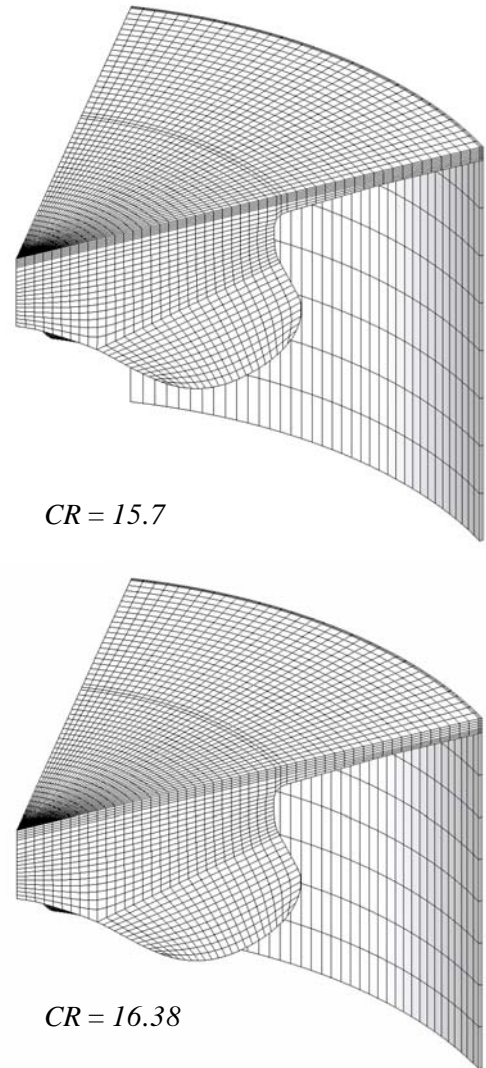


Figure 3. View of the computational grids adopted for the present study: (top) geometrical $CR = 15.7$; (bottom) geometrical $CR = 16.38$ (note the smaller crevice volume height)

blow-by to the crankcase in the CFD simulation, without modifying the actual engine squish height, which is known to have a significant impact on the predicted pollutant emissions, especially CO and UHC.

In the experiments, the "target" squish height used, as reported in Table 1, was estimated by setting a cold clearance height to about 1.04 mm, larger than the target value of 0.88 mm. This difference accounted for the effects of thermal expansion and piston compression. At the 1500 rpm operating condition, the thermal expansion of the piston is mainly caused by ring friction; it was measured to be about 0.31 mm from its cold length. The compliance of the extended piston assembly was directly measured to be $k = 2.2e8$ N/m. However, this value does not include additional compliance effects due to the

connecting rod, any of the bearing clearances, or the base crankcase piston. Thus, an estimated average piston compression value of 0.15 mm was used, corresponding to the effect of a pressure of 60 bar acting onto the piston surface.

In a recent study, Aronsson et al. [15] conducted a detailed experimental campaign to measure deviations from the nominal geometry when operating optical-access engines. In the study it was shown that optical-access piston assemblies undergo significant axial compression during engine operation, leading to actual squish heights at TDC greater than the ones that rigid body slider crank mechanisms would have. In a heavy-duty engine most of the significant increase in squish height (about 1.5 mm at about 80 bar TDC in-cylinder pressure) was observed to be related to thermal expansion of the combustion chamber. This effect was however negligible in a light-duty optical engine that had similar geometrical compression ratio (CR = 16.5) and dimensions (bore x stroke = 81.0 mm x 93.2 mm) as the one studied in the present work. In the engine of Ref. [15], the compressibility of the whole extended optical piston-connecting rod assembly had a significant effect on the overall squish height. The corresponding compressibility behavior was seen to be very well approximated by a linear correlation, with a linear compressibility ratio of about 0.0040 mm/bar, corresponding to a spring-equivalent stiffness constant of about $1.3 \cdot 10^8$ N/m.

In order to verify how much the same phenomenon could be affecting the accuracy of the current computational study, in particular with respect to the amount of volume that had to be added to the combustion chamber to match the motored pressure trace, a static compressible connecting rod assembly model was introduced. In this model, all the inertial and thermal expansion effects are neglected, and the overall compressibility of the extended piston + connecting rod + crank assembly was modeled using a compressible, static spring-like behavior. As the CFD model did not consider detailed modeling of the extended piston assembly, all of the deformation was assigned to the connecting rod. In this way, the actual piston top position is correctly modeled, by considering the compressibility of the whole assembly. However, the linear elastic module assigned to the connecting rod is expected to have a lower value than its physical one, as in the model it represents an “effective” value that incorporates deformations also from the extended piston and the crankshaft joints that can account for more than 50% of the total deformation [15].

Following the observation of Aronsson et al. that the squish height increase was almost linear with in-cylinder pressure for static forces in the range between about 20 kN and 100 kN (i.e., at operating in-cylinder pressures of about 16 bar to 80 bar), the model was defined to follow a simple Hooke’s law spring model:

$$F_{\parallel} = -k \Delta c. \quad (1)$$

The instantaneous force that causes the connecting rod deformation, Δc , is the component - along its axis - of the integral in-cylinder pressure forces on the piston surface:

$$F_{\parallel} = \frac{A_p}{V} \int_V p dV \sqrt{1 - \lambda^2 \sin^2 \vartheta}, \quad (2)$$

where $\lambda = r/c$ is the slider-crank mechanism’s characteristic ratio.

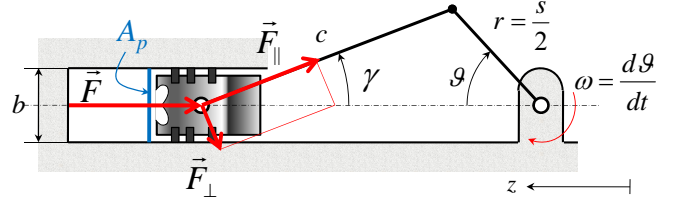


Figure 4. Nomenclature adopted for the slider-crank mechanism with compressible connecting rod model.

The volumetric average of in-cylinder pressure was chosen as the uniform-equivalent pressure acting on the piston, and the other parameters are defined in Figure 4. The derivation of the slider-crank mechanism closure equation, with non-constant connecting rod length, $c = c(t)$, finally yields the instantaneous piston velocity with static compressibility effects as:

$$\frac{dz_p}{dt} = -\frac{s}{2} \omega \sin \vartheta \left(1 + \frac{\tan \gamma}{\tan \vartheta} \right) + \frac{dc}{dt} \cos \gamma. \quad (3)$$

The actual piston velocity can be evaluated from Equation (3), by just adding the instantaneous compression velocity to the rigid slider-crank mechanism law. This is possible because inertial effects are neglected in the model.

The compressible connecting rod model was used to calibrate the engine’s slider-crank movement, and consequently the actual chamber squish height at TDC. As the estimated engine squish height and CR values of Table 1 already partially accounted for piston compressibility, a grid with “geometrical” compression ratio of 16.74, and rigid slider-crank assembly was used as a starting point, by setting the squish height for the CFD model to 0.73 mm. This value was obtained starting from the cold clearance height of 1.04 mm by only subtracting the thermal expansion term of 0.31 mm.

The results were then compared to the motored engine pressure trace; Figure 5 shows that the grid with geometrical compression ratio significantly over-predicted in-cylinder pressure at TDC, by about 7.2 bar, if the compressibility model was not used. Use of the same grid, with the compressible connecting rod model active, instead yielded a very good match with the motored pressure trace, using a spring constant of $k = 4.5 \cdot 10^7$ N/m. This value is about three

times lower than the effective spring constant evaluated on a similar light-duty engine in [15], and about five times lower than the measured compliance of the extended piston only. Also, the squish height at TDC was observed to increase by 0.59 mm, equal to about 48.8% of the geometrical squish height, also leading to an effective compression ratio of about $CR = 15.2$. Finally, at lower pressures during the expansion stroke, recovering the connecting rod length led to a systematic slight over-prediction of the average in-cylinder pressure.

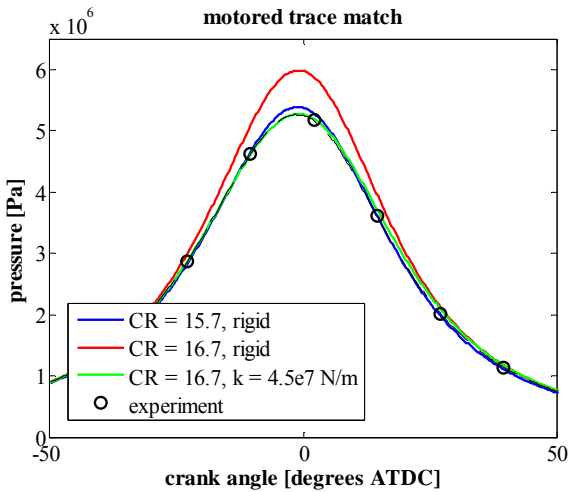


Figure 5. Motored trace match using the compressible connecting rod model and geometrical $CR = 16.7$.

The lower spring constant was identified as the major cause of these deviations from the experimental trace. Such a low value had to be introduced to have the $CR = 16.74$ grid correctly match the peak pressure value at TDC. However, the difference between this value and Ref. [15] suggested that not all of the difference between the measured and predicted pressure traces could be justified by elasticity effects. For this reason, a second analysis was performed keeping the spring constant equal to a reference value, and reducing the geometrical compression ratio by adding volume at the bottom of the top land ring crevice. The value of $k = 1.0 \cdot 10^8$ N/m was set, similar to the stiffness value of [15]. Figure 6 shows that the correct pressure match was found when using a grid with a geometrical compression ratio of about $CR = 16.26$. This configuration appears to be much more physically appropriate since the overall squish height increase (i.e., equivalent connecting rod assembly compression) observed at TDC was of about 0.27 mm, and is of the same order as the elasticity effects measured by Aronsson et al. The effective compression ratio, considering the increased squish height at TDC, was $CR = 15.56$ during motored operation.

Figure 6 shows that both the approaches that consider an artificial increase in combustion chamber volume match the pressure curve very well during the expansion stroke, while they slightly underestimate pressure during compression.

However, the model with exact geometrical compression ratio does a very good job at matching compression stroke pressure, but it over-estimates it during expansion. This observation indicates that charge blow-by to the crankcase has a significant effect on this engine's operation.

The simulation approach with geometrical $CR = 16.26$ and spring constant value $k = 1.0 \cdot 10^8$ N/m was used in the study.

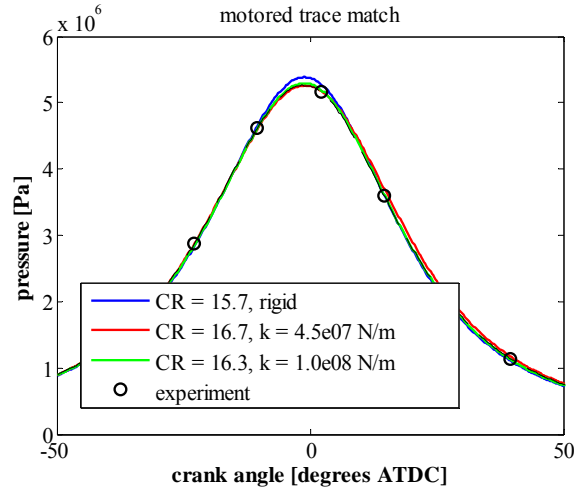


Figure 6. Comparison between the three different grid approaches for motored pressure trace matching: rigid-body model with lowered compression ratio, elastic assembly with geometrical compression ratio, elastic assembly with referenced elasticity and slightly lowered compression ratio.

Local equivalence ratio prediction

Swirl ratio effects

In the experimental campaign Sahoo et al. [11] showed that port-induced swirl affects the overall equivalence ratio distribution. Its interaction with the squish flow also significantly affects the amount and the equivalence ratio of the mixture that enters the squish region and penetrates almost to the cylinder liner. Figure 7 shows predicted vs. experimental comparisons of equivalence ratio for the low-swirl case ($R_s = 1.55$), late after injection and immediately before the main ignition event. The computational model here predicts mixture penetration very well, especially in the squish plane and in the deeper bowl plane, where the jet is correctly seen to reach the center of the bowl.

However, as also pointed out in [9], the differences in equivalence ratio distribution can be due to insufficient mixing. Even if the peak equivalence ratios in the planes are similar to the measured ones, the model does not predict the amount of overly lean mixture forming from the jets and reaching the center of the cylinder. This is confirmed by Figure 8, immediately after the end of injection. At this point,

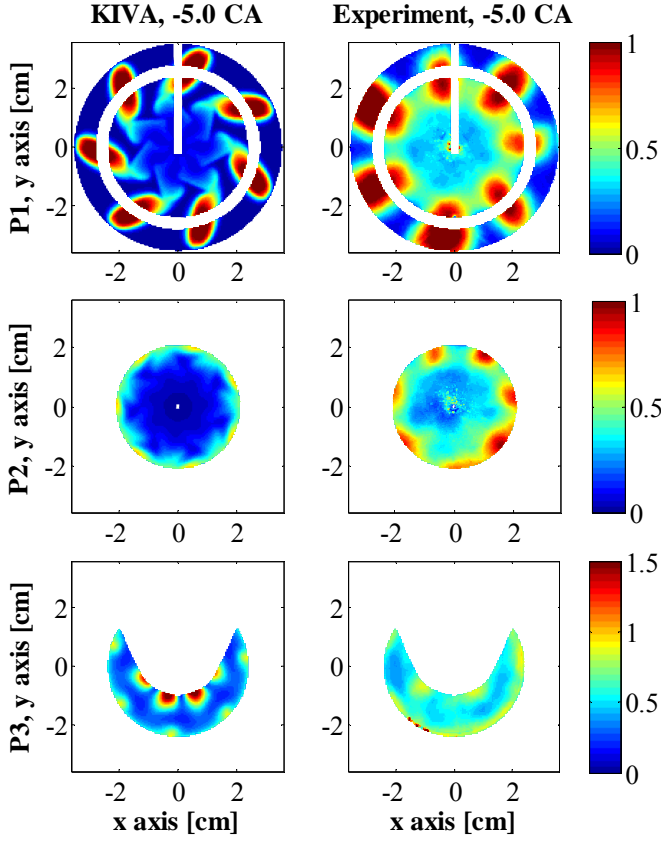


Figure 7. Equivalence ratio distribution comparison for the $R_s = 1.55$, $p_{inj} = 860$ bar case, in planes P1, P2, P3, 5.0 degrees before TDC.

where mixing has not significantly developed yet, spray penetration is already correctly matched. Finally, the simulated plume structure appears to be more twisted by the swirling motion than the PLIF images show, i.e., an almost radially-aligned jet can be seen from the experiments.

The computational model consistently showed the same behavior up to the largest swirl ratio (Figure 9 and Figure 10, $R_s = 4.50$): as the swirl ratio increased, the KIVA-simulation-predicted equivalence ratios in the P2 and P3 planes were still very accurate, but smaller spray penetration into the squish region was predicted by the code. However, in this case (Figure 9), the greater mixing that led to lean equivalence ratios in the upper central part of the combustion chamber was better represented, as also measured in plane P1.

Swirling flow structure

The different spray deflection is correlated with the under-predicted spray penetration, as greater air entrainment into the jet due to the flow swirl could account for lower radial penetration. For this reason, the swirling vortex structure in the simulations was compared to the PIV measurements of Petersen and Miles [24] on the same engine. In their analysis,

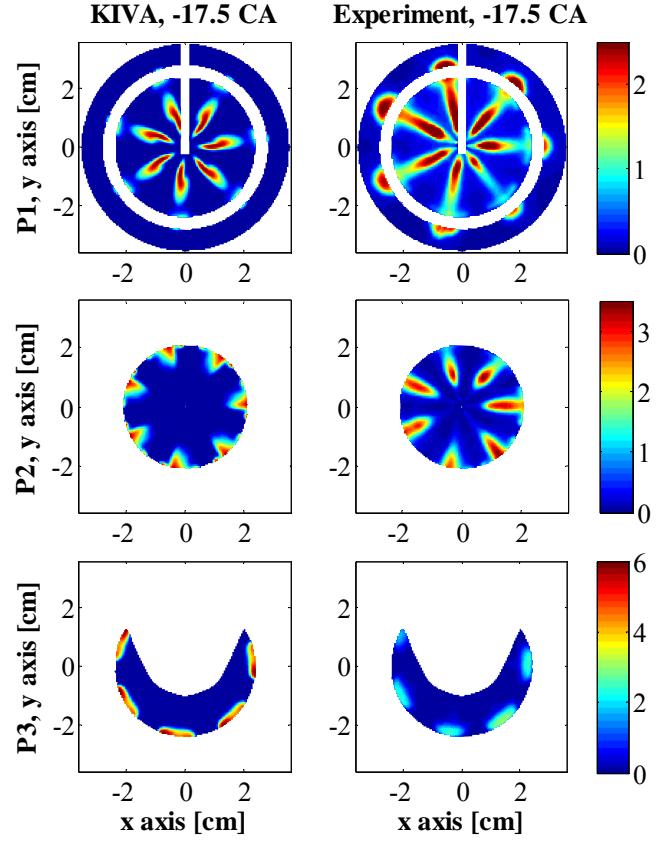


Figure 8. Equivalence ratio distribution comparison for the $R_s = 1.55$, $p_{inj} = 860$ bar case, in planes P1, P2, P3, 17.5 degrees before TDC.

it was shown that the macroscopic swirling structure does not change significantly with the overall vortex momentum, and that the tangential velocity profile versus the radial coordinate could be well approximated by a Bessel function, with shape coefficient $\alpha = 2.20$.

In Figure 11 a comparative view of the simulated and measured tangential velocity profiles in the optical engine is given. As for the experiments [24] the simulated velocity profiles were taken at a fixed reference plane, 3 mm below the firedeck. The first plot refers to the baseline operating conditions, with $R_s = 2.20$, at crank angles prior to the start of injection; the second one refers to a fixed measurement timing about 11.4 crank angle degrees prior to the injection, and compares different port-induced swirl ratios. This latter plot clearly shows a very good consistency between the KIVA prediction and the experimental tangential velocity measurements, indicating that the code is accurately predicting the swirl velocity distribution in the upper cylinder and squish volume. In contrast, the comparison at different crank angles shows that the computational model predicts an accelerated swirling flow in the central region of the cylinder near TDC, as would be expected as high-angular momentum from the

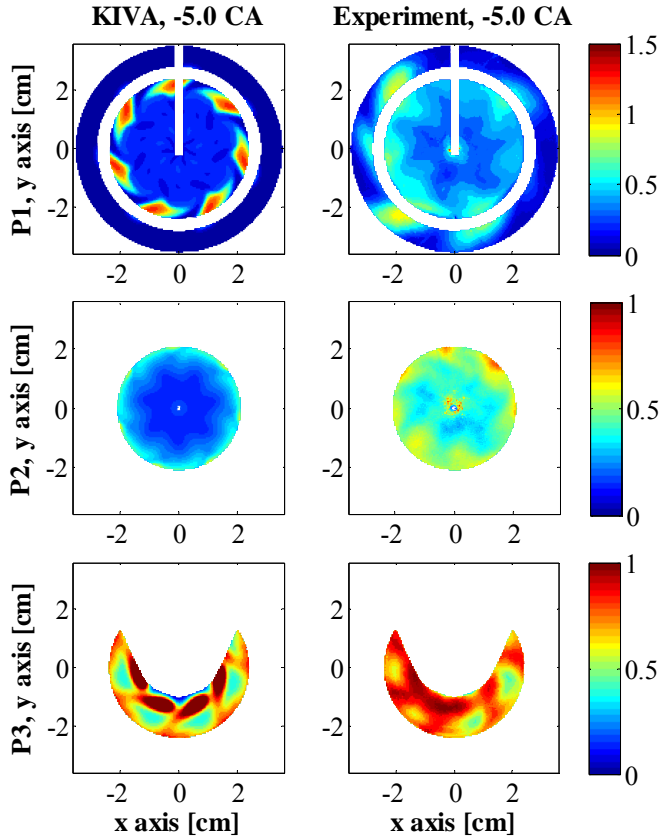


Figure 9. Equivalence ratio distribution comparison for the $R_s = 4.50$, $p_{inj} = 860$ bar case, in planes P1, P2, P3, 5.0 degrees before TDC.

squish volume is forced inward. The absence of this feature in the experimental data suggests that missing geometrical

features in the computational grid, such as the valve recesses on the cylinder head and the cut-outs on the piston surface in the squish region are attenuating the angular momentum within the squish volume, leading to smaller tangential velocities when the piston approaches TDC.

Injection pressure effects

As pointed out in the experimental campaign [11], injection pressure has a large impact on engine-out emissions due to the stronger jet penetration, and leaner mixture formation in the near-nozzle region due to increased air entrainment into the jet and greater stratification near the bowl rim. Figure 12 and Figure 13 show the experimental versus numerical comparisons of local equivalence ratios at the three

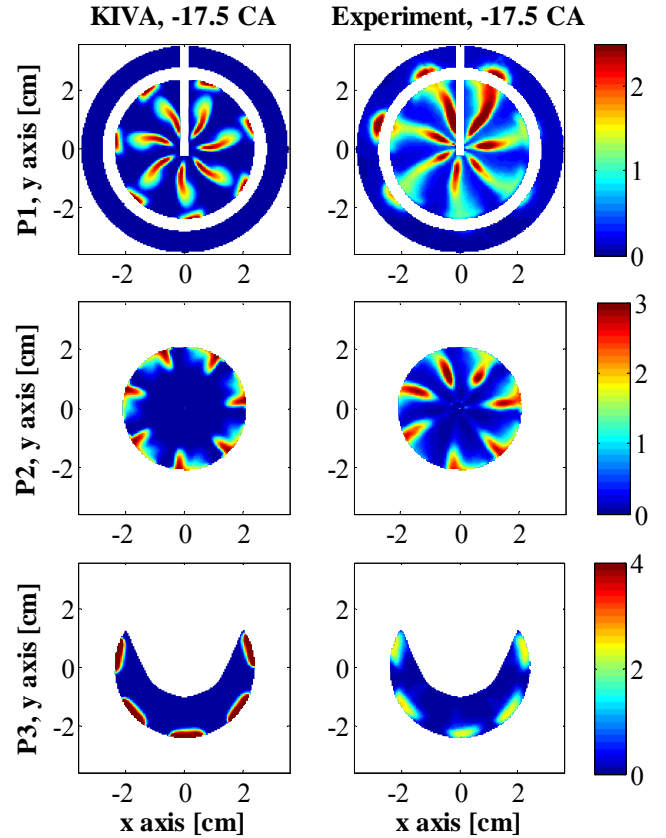


Figure 10. Equivalence ratio distribution comparison for the $R_s = 4.50$, $p_{inj} = 860$ bar case, in planes P1, P2, P3, 17.5 degrees before TDC.

experimental planes, and at the two extremes of injection pressure, i.e., $p_{inj} = 500$ bar and $p_{inj} = 1220$ bar, respectively.

The comparisons are at CA = -5.0 degrees ATDC, about 15 degrees after the end of injection and before the main ignition event. In the low-pressure case, the KIVA model shows an under-predicted penetration of the fuel-air mixture both into the squish region and into the bowl. This phenomenon is not however observed for the high injection pressure case. At $p_{inj} = 500$ bar, lower jet momentum leads to less over-lean mixture in the central part of the upper plane (P1), partially compensating for lack of mixing in this zone, but no fuel vapor at all is predicted to enter the squish region

This same effect is also captured at plane P2, where the jet impacts against the piston bowl rim. Near the wall, an almost stoichiometric mixture is formed. At the highest injection pressure, $p_{inj} = 1220$ bar instead, the kinetic energy introduced by the spray jet is higher, and the KIVA model very well

matches the measured penetration into the squish region of the upper part of the jet, after its impact against the piston bowl rim..

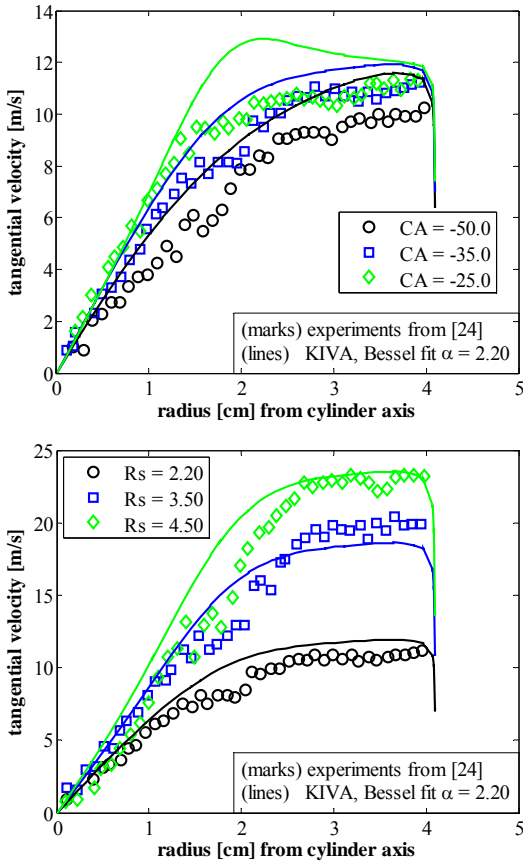


Figure 11. Predicted (KIVA) and experimental tangential velocity profiles at (top) different crank angles, swirl ratio $R_s = 2.2$; (bottom) different swirl ratios, at -35 degrees ATDC.

In this case, a mixture with very lean equivalence ratio of $\phi < 0.5$ is predicted to be formed in the central part of the upper plane, still suffering for lack of mixing, more for the fuel vapor amount than for its distribution. Computational modeling also predicts well the mixture distribution in the inner bowl plane P3. Here, at the higher injection pressure, the lower portion of the jet penetrates further into the bowl, and its leading edge travels along the bowl surface, back towards the central, near-axis region, where it can be seen rising back up into the measurement plane. This farthest part of the jet however does not reach back to the central regions of plane P2, where a good match is seen only for the near-stoichiometric mixture at the bowl rim caused by fuel impingement. The central region in this plane shows the most significant deviations from the corresponding PLIF measurements, which exhibit no fuel vapor. However, the present results confirm the observations in [11] that the probability of finding over-lean mixture ($0.2 \leq \phi \leq 0.5$) just before the main ignition event is greater in this plane, and in

the central region of plane P1. Also, the probability of finding over-lean mixtures in the deeper bowl region is confirmed to be lower at high injection pressures.

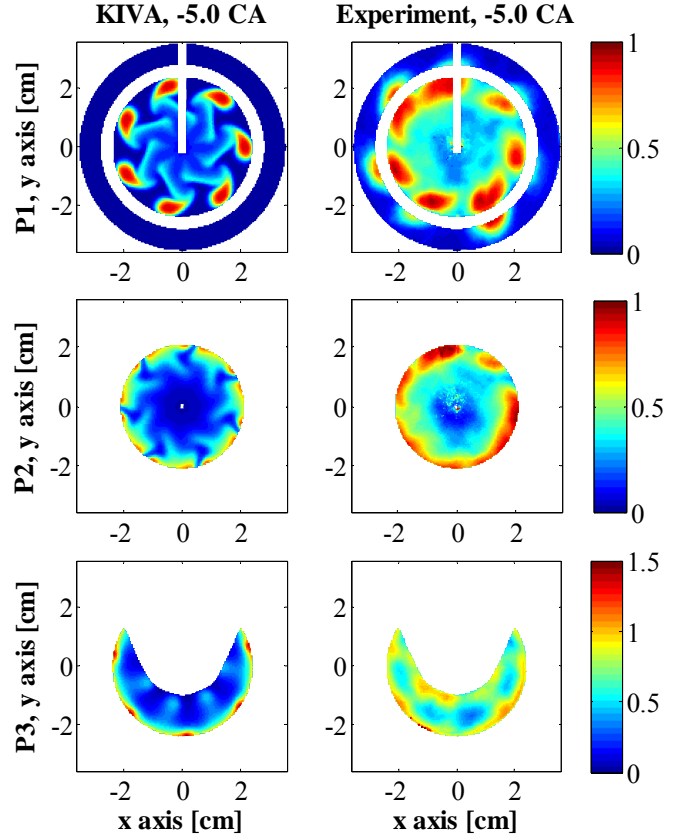


Figure 12. Equivalence ratio distribution comparison for the $R_s = 2.20$, $p_{inj} = 500$ bar case, in planes P1, P2, P3, 5.0 degrees before TDC.

Mixture stratification comparison

A quantitative comparison of the model's capability to represent the equivalence ratio distribution in the combustion chamber just before the main ignition is given in Figure 14 and Figure 15. The two bar graphs represent cumulative azimuthal equivalence ratio distributions as a function of the cylinder radius, at the three PLIF planes, and for the lowest and highest injection pressure cases, respectively. The images' pixel data were used to gather the information. All pixels with equivalence ratio $\phi > 0.1$ have been sorted as a function of their distance from the cylinder axis, and then binned into a number of equally-spaced ranges. Seven equivalence ratio ranges were selected to identify overly-lean (blue colors), lean (green), near-stoichiometric (yellow), and rich (red) regions. This format presents the equivalence ratio stratification in each zone, thus characterizing the mixing, and its trend within

the planes. In Figure 14, for example, the qualitative prediction of equivalence ratio distribution in planes P1 and P2 is confirmed. Apart from the absence of fuel vapor entering the squish region, the distribution of equivalence ratios in plane P1 matches well the experimental figure, and shows

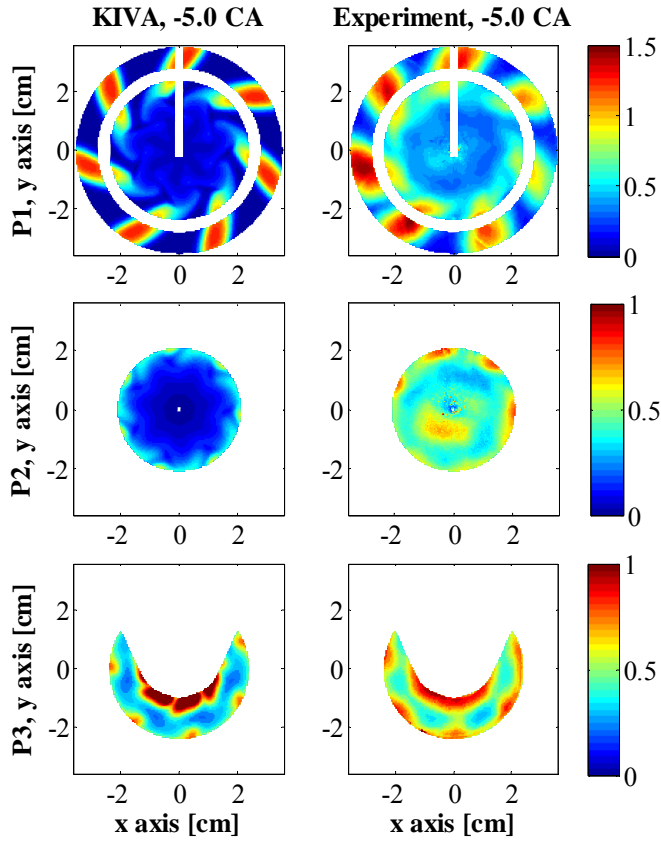


Figure 13. Equivalence ratio distribution comparison for the $R_s = 2.20$, $p_{inj} = 1200$ bar case, in planes P1, P2, P3, 5.0 degrees before TDC.

the dominant lean or overly-lean mixtures in the central region, and an overall very low stratification. A unique region of slightly lean mixtures is identified as the zone just above the piston bowl rim, where part of the impinged jet is deflected towards the squish region. In this region the predicted equivalence ratios are very similar to the experimental values, thus the distribution shows that the amount of overly-lean mixture with $\phi \leq 0.5$ is well predicted up to 2.7 cm from the axis, i.e., until the piston bowl rim. The bowl rim plane, P2, confirms agreement in the equivalence ratio distribution, and lack of mixing towards the central zone. As with the experimental measurements, most of the mixture near the bowl rim is near-stoichiometric or slightly lean (70%). In the central part of the cylinder, the mixture is instead completely overly-lean. The model is not able to predict very lean mixture ($\phi \leq 0.10$) to be formed at the cylinder axis, but also in the experimental measurement most of the mixture in this zone is very lean ($0.1 \leq \phi \leq 0.25$) and the

absolute error is small. Plane P3 shows perhaps the greatest deviations from the experimental measurements. There is good agreement in the outer-wall region, but predicting overly-lean equivalence ratios in the central part, where instead the PLIF image shows slightly lean or even almost-

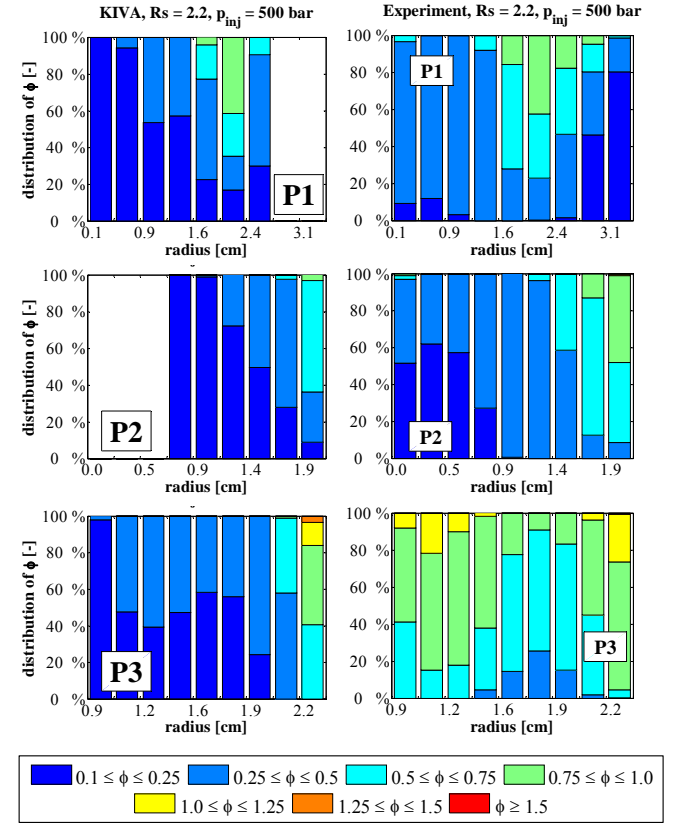


Figure 14. Predicted (left) vs. experimental (right) equivalence ratio distributions at planes P1, P2, P3, immediately before the main ignition event (CA = -5.0 degrees ATDC). Swirl ratio $R_s = 2.20$, injection pressure $p_{inj} = 500$ bar.

stoichiometric values. This is probably due to the measured greater penetration of the jet within the bowl, where it can be seen rising up through the measurement plane again within the central part of the bowl.

Figure 15 shows the equivalence ratio distribution at injection pressure $p_{inj} = 1220$ bar, which is more typical of high-pressure diesel injection. It should be noted that this injection pressure is closer to values at which the spray models and their constants have been validated. Here, the computational model does a much better job at predicting the overall equivalence ratio distribution in the combustion chamber. In plane P1, the penetration of the fuel vapor into the squish region is correctly predicted at the bowl rim radius, and forms a slightly rich mixture. A very similar penetration towards the cylinder liner is also seen. At the piston bowl rim edge, generally lean equivalence ratios are predicted, as also confirmed by the

experimental images. Slightly lower equivalence ratios are seen in the computational model in the central region. It has been noted that liquid-spray induced scattering of the laser light could lead to a slight overestimation of the equivalence ratio [11], very close to the cylinder axis; however, this effect

at the highest pressures, resulting in a greater probability to find overly-lean regions in the central part of the cylinder.

Study of fired engine operation

Injection pressure effects on fired engine operation

In the experimental study three different injection pressures $p_{inj} = 500, 860, 1220$ bar were tested at the reference operating condition with swirl ratio $Rs = 2.2$. It was observed that at this very low load increasing the injection pressure lowered the peak rate of heat release as a consequence of a more stratified equivalence ratio distribution that is caused by a less favorable mixing process. This also affected pollutant emissions due to increased jet penetration into the squish volume that led to higher engine-out UHC and CO.

Figure 16 shows the experimental vs. numerical average in-cylinder pressure and apparent heat release rate (AHRR). The plots show that the model is able to reliably predict the correct ignition delays for all cases, including both the low-temperature heat release starting at about -15 degrees ATDC, and the main ignition event occurring around -5.0 degrees. In particular, the model matches reasonably well the peaks of AHRR, especially at $p_{inj} = 860$ bar and $p_{inj} = 1220$ bar, suggesting that also wall heat transfer has been correctly captured. At the lowest injection pressure, as seen by the comparison of local equivalence ratios immediately before the main ignition event, the model predicts penetration both into the piston bowl (plane P3) and into the squish region (plane P1). This leads to a good agreement with the experiments in terms of combustion duration, but a slight underestimation of the AHRR peak is seen. A summary of the predicted engine-out emissions is also reported in Table 4.

The generally good reliability shown by the model allowed it to be used to explore a wider range of operating injection pressures. As shown in Figure 17, measured injection rates at the three injection pressures used in the PLIF experiments, were used to extrapolate the injection rates to higher pressures. The total injected mass was kept constant and equal to $m_{inj} = 8.8$ mg, while the total injection time and the injection rate shape were determined by calculating, point-by-point in time, the polynomial curve that interpolates between the three corresponding experimental points.

Figure 18 shows the predicted in-cylinder pressure and wall heat transfer rate, for injection pressures ranging from 500 to 2000 bar. The plots show that higher injection pressures lead to significantly increased wall heat transfer rates, starting at SOI and ending before TDC. As Figure 19 shows, the increase in wall heat transfer at the highest injection pressures is related to the higher jet velocities impinging against the piston bowl rim, and a concurrent increase in impact area. As shown in Figure 20, increased injection pressures also dramatically affect the jet penetration into the squish volume.

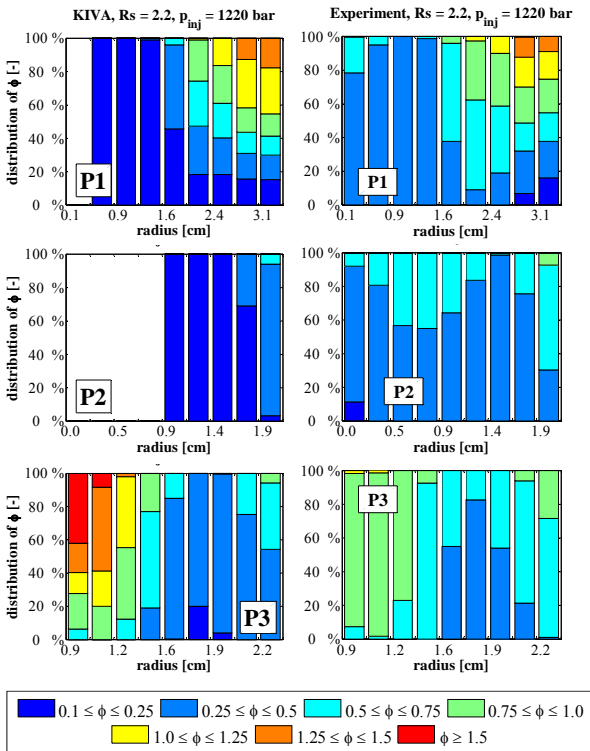


Figure 15. Predicted (left) vs. experimental (right) equivalence ratio distributions at planes P1, P2, P3, immediately before the main ignition event (CA = -5.0 degrees ATDC). Swirl ratio $Rs = 2.20$, injection pressure $p_{inj} = 1220$ bar.

cannot account for the whole amount of combustible mixture measured in that zone, that the simulation does not capture because of its general trend toward reduced mixing throughout the jet development. Finally, the equivalence ratio distribution in plane P3 shows a very good agreement at the bowl walls, even though the mixture in the central region appears to be more stratified; here, rich equivalence ratios are seen, suggesting for a lack of penetration of the farthest jet part back into the central part of plane P2.

Overall, even with some deficiencies in predicting the jet penetration far into the bowl and the mixing in the central part of the cylinder, the model was able to capture very well the trend that higher injection pressures lead to more stratified mixtures within the upper squish volume plane.

Also, the greater jet penetration and deflection into the bowl and towards the bowl pip at the cylinder axis was confirmed by the model to provide greater equivalence ratios in this zone

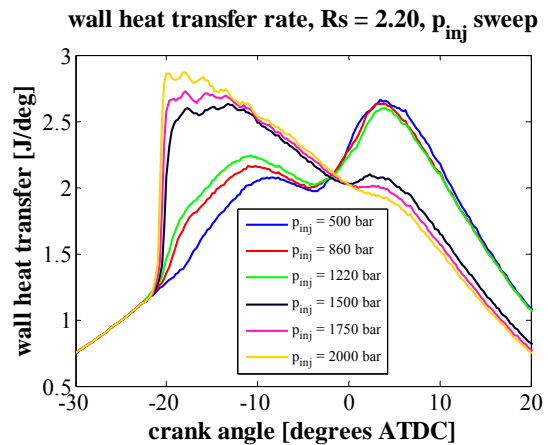
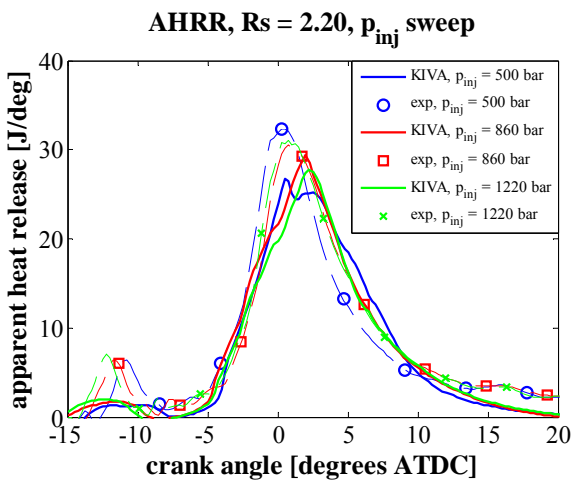
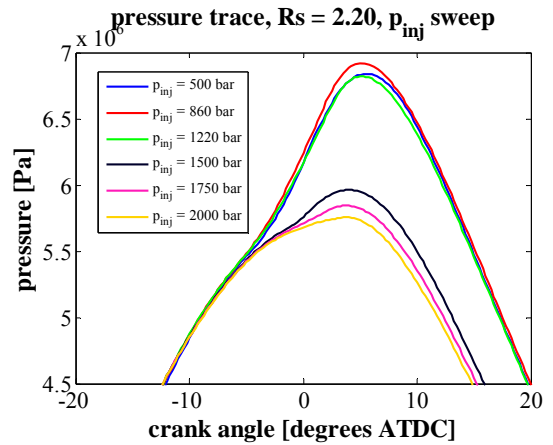
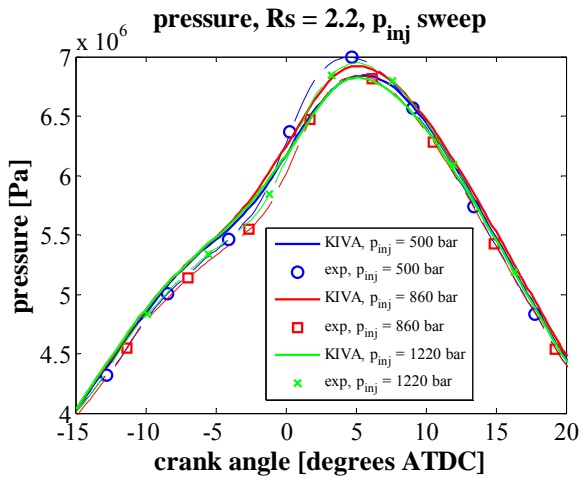


Figure 16. Fired cases comparison: average in-cylinder pressure traces and apparent rate of heat release. KIVA simulations (solid lines) vs. experiments (dashed lines with marks). Swirl ratio $Rs = 2.2$, injection pressure sweep.

Figure 18. Cylinder pressure and total in-cylinder wall heat transfer. Injection pressures $p_{inj} = 1500$ bar (left), reference $p_{inj} = 860$ bar (right).

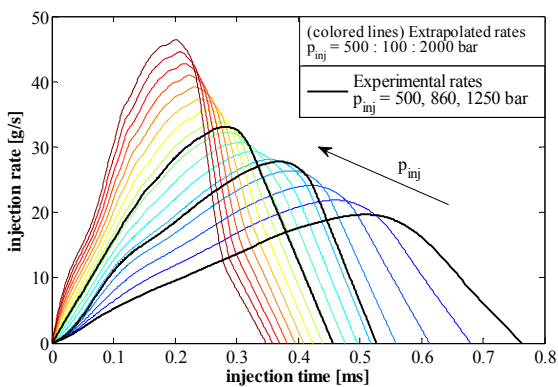


Figure 17. Extrapolated injection rate shapes for the Bosch CRIP 2.2 injector, injected mass $m_{inj} = 8.8$ mg. Thick lines represents experimental rate shapes at 500, 860, 1250 bar. Thin lines represent extrapolated rates from 500 to 2000 bar.

At $p_{inj} = 1500$ bar far before ignition the jet reaches the cylinder liner, and a non-negligible amount of fuel vapor enters the top ring-land crevice. The concurrent presence of these two effects prevents the mixture from undergoing complete ignition for this very low load case at injection pressures starting from 1500 bar.

Swirl ratio effects on fired engine operation

In the experimental campaign the main ignition event was observed to occur earlier at higher swirl ratios. This is due to a greater amount of premixed combustible mixture ($0.5 \leq \phi \leq 1$) becoming available due to improved mixing. In the experiments the only case that did not follow this trend was at $Rs = 1.55$. The overall ignition timing was observed to be almost equal to the timing at $Rs = 3.5$. The predicted KIVA pressure and apparent heat release rate traces in Figure 21 show very similar ignition timings that however depend inversely on swirl ratio: the computational model predicts slightly delayed ignition at higher swirl ratios.

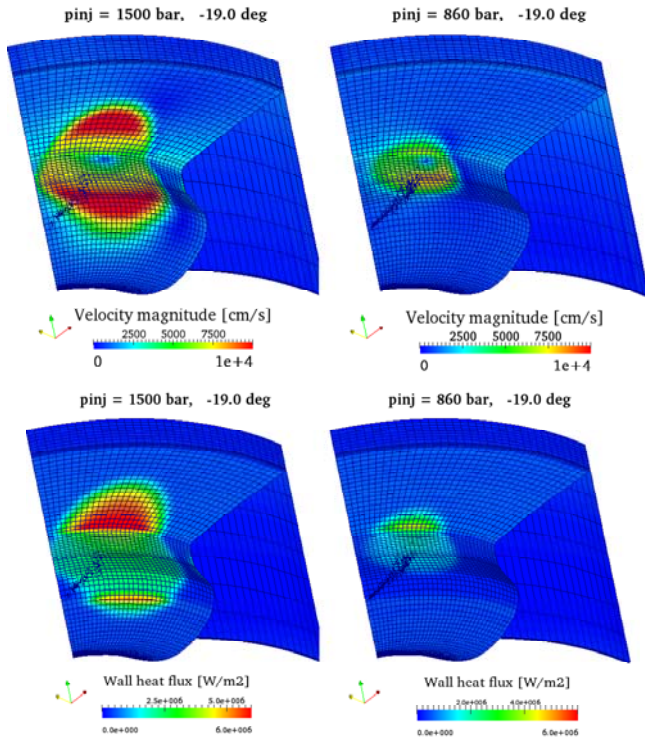


Figure 19. Jet impact velocity and wall heat flux comparison at the end of injection (CA = -19 deg ATDC). Injection pressures $p_{inj} = 1500$ bar (left), reference $p_{inj} = 860$ bar (right).

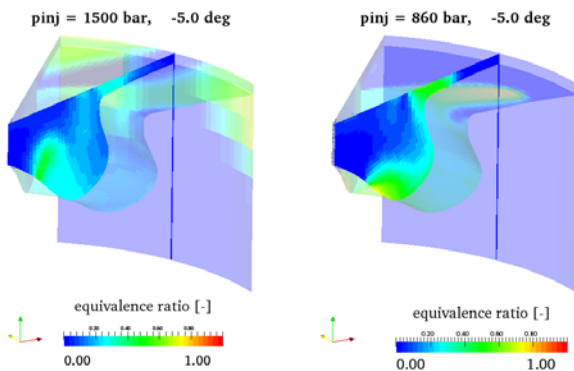


Figure 20. Equivalence ratio comparison late after the end of injection (CA = -5 deg ATDC). Injection pressures $p_{inj} = 1500$ bar (left), reference $p_{inj} = 860$ bar (right).

As highlighted in Figure 22, the increase in total wall heat transfer is also significant at higher swirl ratios, and increases about 13.2% from $R_s = 1.55$ to $R_s = 3.5$ (total predicted heat exchanged at the walls at EVO was 104.4 J and 118.2 J, respectively). To quantify the effects of swirl and wall heat transfer these two cases were further analyzed.

Table 4. Measured [11] vs. predicted engine-out emissions for the swirl ratio and the injection pressure sweeps.

p_{inj} [bar]	R_s	UHC [g/kg _f]		CO [g/kg _f]		NO _x [mg/kg _f]	
		KIVA	Exp.	KIVA	Exp.	KIVA	Exp.
p_{inj} sweep							
500	2.2	81.1	10.5	195.3	96.7	57	46
860	2.2	71.0	10.5	207.1	117.8	55	34
1220	2.2	85.0	11.0	250.2	130.0	35	30
R_s sweep							
860	1.55	70.1	8.9	216.5	96.2	47	32
860	2.2	71.0	10.5	207.1	117.8	55	34
860	3.5	63.2	12.3	188.6	95.3	46	39
860	4.5	83.7	11.6	213.4	87.6	25	40

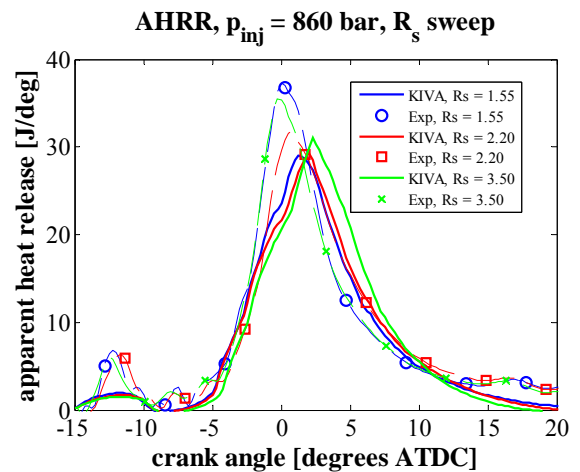
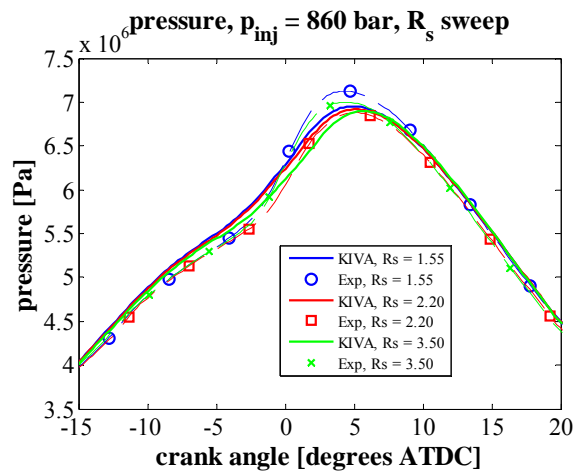


Figure 21. Fired cases comparison: average in-cylinder pressure traces and apparent rate of heat release. KIVA simulations (solid lines) vs. experiments (dashed lines with marks). Injection pressure $p_{inj} = 860$ bar, swirl ratio sweep.

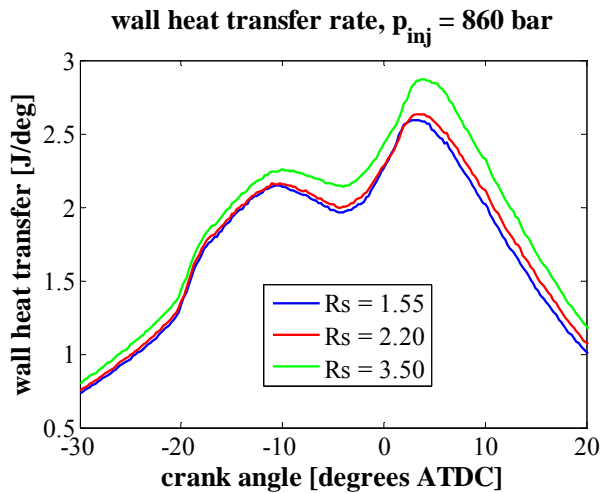


Figure 22. Fired cases comparison: KIVA wall heat transfer rate traces, $p_{inj} = 860$ bar, swirl ratio sweep.

In particular, it was observed [11] that they have almost the same combustion efficiency (less than 1% difference), but the $Rs = 3.5$ case showed almost a 5% decrease in overall heat release. The simulations catch very well this behavior, as the corresponding simulated cumulative apparent heat release values are 218.4 J and 206.3 J, respectively (-4.3% for the $Rs = 3.5$ case), while the overall heat releases due to combustion are 350.3 J and 351.3 J, respectively (about 0.6 % discrepancy). Both the experiments and the simulations thus confirm that the impact of wall heat transfer is significant at very high swirl ratios. Also, the critical dependency of the ignition timing at very low loads on in-cylinder spray-flow field interactions, and on mixing and heat transfer is also confirmed by the simulations.

In the model, the main ignition event appears to be more affected by wall heat transfer than by mixing, even when the local equivalence ratios agreed well at all swirl ratios, and especially at the latest crank angle, CA = -5.0 deg ATDC, immediately before the main ignition event. This suggests that further analysis should focus on the impact of the flow field on the differences among the spray jets. It was observed in the previous study by Dempsey et al. [9] that the flow field structure at IVC is almost destroyed during compression. Geometrical details, such as valve recesses in the cylinder head and cut-outs on the piston surface, can be relevant especially for their influence on the swirling motions into the squish region, and they could account for different nozzle-by-nozzle spray plume impingement and penetrations.

CONCLUDING REMARKS

A recent experimental study investigated the role of injection pressure and swirl ratio on local mixture preparation and its effect on combustion characteristics and pollutant emissions in a light-duty, optical diesel engine operated in an early-

injection, low-load and low-temperature combustion mode. The aim of the present work was to further validate engine CFD simulations, and to use the computer model to understand and explore the role of wall heat transfer on combustion, when high injection pressures or high swirl ratios are employed.

The comparison with a detailed set of PLIF measurements of local mixture formation and distribution after injection in a non-reacting gas confirmed the reliability of the computer model at seven different operating conditions including a range of swirl ratios from $Rs = 1.55$ to $Rs = 4.50$ and injection pressures from $p_{inj} = 500$ bar to $p_{inj} = 1220$ bar. In the study the following conclusions were reached.

- An elastic model for the extended piston – connecting rod assembly of the optical engine was tested. It was found that when using rigid slider-crank movement, the CFD model could not correctly capture the motored engine operation, and the peak pressure at TDC was overestimated even after reducing the geometrical compression ratio. Use of the new model could account for an increase in squish height at TDC of about 0.27 mm in motored engine operation, leading to an excellent agreement with the experimental pressure trace. An increase of crevice volume was considered to account for mass blow-by to the crankcase. This suggests that the incorporation of an elastic model is useful for better incorporating compressibility and blow-by effects on engine operation;
- The comparison of the model predictions with the PLIF measurements, and in particular the differences observed between the measured and the computed equivalence ratio distributions, confirmed the crucial role of mixing on ignition. The model reliably predicted mixture dynamics and equivalence ratio stratification before the main ignition event. Jet penetration into the squish region was pretty well matched, despite under-prediction occurring especially at low injection pressures due to, at least in part, greater swirl-induced deflection of the spray jet in the upper region of the combustion chamber. The equivalence ratio distribution late after injection appeared to suffer from lack of appropriate mixing. This points out the need to incorporate more refined geometrical details about the combustion chamber, such as valve recesses and cut-outs, and to study their effects on the bulk flow motion and on the jet dynamics after impingement against the piston bowl rim.

For fired engine operation, the study compared the modeling results to average in-cylinder pressure and apparent rates of heat release with the following conclusions:

- At higher swirl ratios, wall heat transfer increased significantly, leading to slight delays in predicted ignition timings. However, the experimental measurements had shown that improved mixing led instead to ignition

advances. The dependency of the results on heat transfer and local mixing suggests that more detailed modeling of the combustion chamber geometry would also help to understand how jet-to-jet behavior changes due to different spray impingement and tangential velocities in the upper part of the combustion chamber affect the overall combustion characteristics;

- The injection pressure plays a major role on the combustion development. It was observed that increased impact area and greater momentum of the spray jet led to a significant increase of wall heat transfer and mixture stratification, and a corresponding delay in ignition timing. Also, the modeling showed that greater penetration into the squish region, and eventually into the crevice volume, can lead to misfiring conditions at higher injection pressures.

The present CFD model proved to be reliable and suitable to simulate low-load and low-temperature combustion operation in a light duty engine. Further work will focus on the improvement of the model accuracy, especially in the squish volume region, where the formation of overly-lean mixtures controls pollutant formation, and is the fundamental source of CO and unburned hydrocarbons.

REFERENCES

1. Lu, X., Han D., Huang Z., "Fuel design and management for the control of advanced compression-ignition combustion modes", *Progress in Energy and Combustion Science* 37(6), 741-783, 2011.
2. Herner, J.D., Hu, S., Robertson, W.H., Huai, T., Oliver Chang, M.C., Rieger, P., Ayala, A., "Effect of Advanced Aftertreatment for PM and NO_x Reduction on Heavy-Duty Diesel Engine Ultrafine Particulate Emissions", *Environmental Science and Technology* 45, 2413-2419, 2011.
3. Noehre, C., Andersson, M., Johansson, B., and Hultqvist, A., "Characterization of Partially Premixed Combustion", SAE technical paper 2006-01-3412, 2006, doi:10.4271/2006-01-3412.
4. Ekoto, I. W., Colban, W. F., Miles, P. C., Park, S. W., Foster, D. E., Reitz, R. D., Aronsson, U., and Andersson, O., "UHC and CO Emissions Sources from a Light-Duty Diesel Engine Undergoing Dilution-Controlled Low-Temperature Combustion", SAE technical paper 2009-24-0043, 2009, doi:10.4271/2009-24-0043.
5. Musculus, M. P. B., Lachaux, T., Pickett, L. M., and Idicheria, C. A., "End-of-Injection Over-Mixing and Unburned Hydrocarbon Emissions in Low Temperature Combustion Diesel Engines", SAE technical paper 2007-01-0907, 2007, doi:10.4271/2007-01-0907.
6. Petersen, B., Miles, P., Ekoto, I., "An Investigation into the Effects of Fuel Properties and Engine Load on UHC and CO Emissions from a Light-Duty Optical Diesel Engine Operating in a Partially Premixed Combustion Regime", *SAE Int. J. Engines* 3(2), 38-55, 2010, doi: 10.4271/2010-01-1470.
7. Petersen, B., Miles, P., Ekoto, I., "Optical Investigation of UHC and CO Sources from Biodiesel Blends in a Light-Duty Diesel Engine Operating in a Partially Premixed Combustion Regime", *SAE Int. J. Engines* 3(1), 414-434, 2010, doi:10.4271/2010-01-0862.
8. Petersen, B., Sahoo, D., Miles, P., "Equivalence Ratio Distributions in a Light-Duty Diesel Engine Operating under Partially Premixed Conditions", *SAE Int. J. Engines* 5(2), 526-537, 2012, doi: 10.4271/2012-01-0692.
9. Dempsey, A., Wang, B., Reitz, R., Petersen, B. et al., "Comparison of Quantitative In-Cylinder Equivalence Ratio Measurements with CFD Predictions for a Light Duty Low Temperature Combustion Diesel Engine," *SAE Int. J. Engines* 5(2):2012, doi:10.4271/2012-01-0143.
10. Sahoo, D., Petersen, B., and Miles, P., "Measurement of Equivalence Ratio in a Light-Duty Low Temperature Combustion Diesel Engine by Planar Laser Induced Fluorescence of a Fuel Tracer," *SAE Int. J. Engines* 4(2), 2312-2325, 2011, doi:10.4271/2011-24-0064.
11. Sahoo, D., Petersen, B. R., Miles, P. C., "The Impact of Swirl Ratio and Injection Pressure on Fuel-Air Mixing in a Light-Duty Diesel Engine", 2012 Spring Technical Conference of the ASME Internal Combustion Engine Division, Torino (Italy), May 6-9, 2012.
12. Amsden, A. A., "KIVA-3V: A block-structured KIVA program for engines with vertical or canted valves", 1997, Los Alamos National Laboratory Report LA-13313-MS.
13. Amsden, A. A., "KIVA-3V, Release 2, improvements to KIVA-3V", 1999, Los Alamos National Laboratory Report LA-UR-99-915.
14. Sauter, J.W., Lee, C.W., Ra, Y., Reitz, R.D., "Model Parameter Sensitivity of Mixing and UHC/CO Emissions in a PPCI, Low-Load Optical Diesel Engine", SAE Technical Paper 2011-01-0844, 2011, doi: 10.4271/2011-01-0844.
15. Aronsson U., Solaka H., Lequien G., Andersson O., Johansson, B., "Analysis of Errors in Heat Release Calculations Due to Distortion of the In-Cylinder Volume Trace from Mechanical Deformation in Optical Diesel Engines", *SAE Int. J. Engines* 5(4):2012, doi:10.4271/2012-01-1604.
16. Beale, J. C. and Reitz, R. D., Modeling Spray Atomization with the Kelvin-Helmholtz/Rayleigh-Taylor hybrid model, *Atomization and Sprays*, 1999, Volume 9, pp. 623-650.
17. Baumgarten, C., *Mixture Formation in Internal Combustion Engines* (2006), Springer, pp. 116.
18. Abani, N., Munnannur, A., and Reitz, R. D., Reduction of Numerical Parameter Dependencies in Diesel Spray Models, *Journal of Engineering for Gas Turbines and Power*, 2008, Vol. 130 032809.
19. O'Rourke, P. J. and Amsden, A. A., A Spray/Wall Interaction Submodel for the KIVA-3 Wall Film Model, SAE 2000-01-0271.

20. Ra, Y. and Reitz, R. D., A vaporization model for discrete multi-component fuel sprays, *International Journal of Multiphase Flow*, 2009, 35, 101-117.
21. Han, Z. and Reitz, R. D., Turbulence Modeling of Internal Combustion Engines Using RNG k-e Models, *Combustion Science and Technology*, 1995, Vol. 106, pp. 267-295.
22. Ra, Y. and Reitz, R.D., “A reduced chemical kinetic model for IC engine combustion simulations with primary reference fuels”, *Combustion and Flame*, 2008, Vol. 155(4), 713-738.
23. Perini, F., Galligani, E., Reitz, R.D., “An Analytical Jacobian Approach to Sparse Reaction Kinetics for Computationally Efficient Combustion Modeling with Large Reaction Mechanisms”, *Energy&Fuels* 26 (8), 4804-4822, 2012.
24. Petersen, B. and Miles, P. C., “PIV Measurements in the Swirl-Plane of a Motored Light-Duty Diesel Engine”, *SAE International Journal of Engines*, Vol. 4(1), 1623-1641.
25. Sauter, J. W., Lee, C. W., Ra, Y., and Reitz, R. D., Model Parameter Sensitivity of Mixing and UHC/CO Emissions in a PPCI, Low-Load Optical Diesel Engine, SAE 2011-01-0844.

CONTACT

Federico Perini
Engine Research Center
University of Wisconsin-Madison
Madison, WI 53706-1609, USA
perini@wisc.edu

ACKNOWLEDGMENTS

This material is based on work supported by the Department of Energy Sandia Laboratories.

The authors wish to thank Bishwadipa Das Adhikary for providing the experimental injection rate data at 1250 bar, and for the useful discussions.